iScience

CellPress
OPEN ACCESS

Article

AMPylation profiling during neuronal differentiation reveals extensive variation on lysosomal proteins

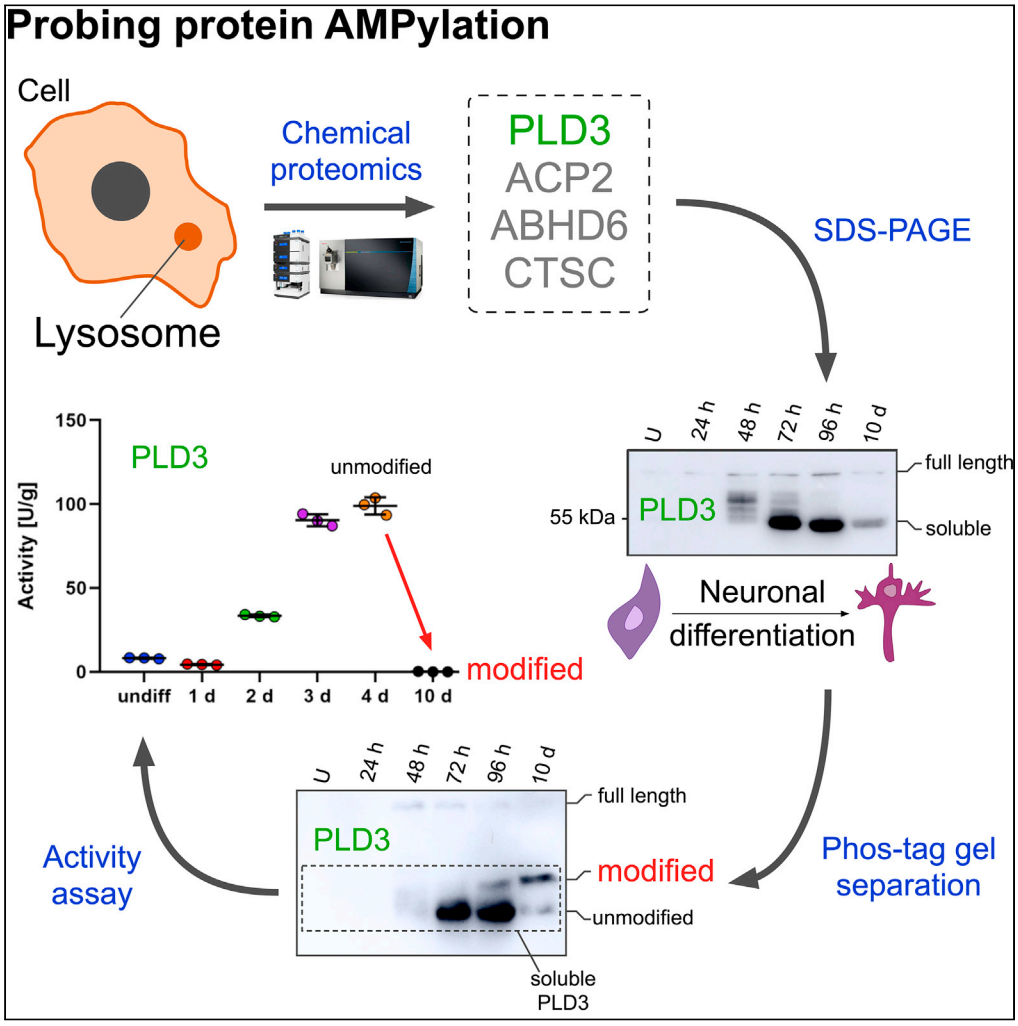

Tobias Becker, Cedric Cappel, Francesco Di Matteo, ..., Silvia Cappello, Markus Damme, Pavel Kielkowski

pavel.kielkowski@cup.lmu.de

Highlights

Profiling of AMPylation during neuronal differentiation

AMPylation is a potential PTM of luminal lysosomal proteins

Phos-tag gel enables the separation of non-AMPylated and AMPylated proteins

The modified lysosomal soluble form of PLD3 increases during neuronal maturation

Becker et al., iScience 24, 103521
December 17, 2021
https://doi.org/10.1016/j.isci.2021.103521

iScience

CellPress
OPEN ACCESS

Article

AMPylation profiling during neuronal differentiation reveals extensive variation on lysosomal proteins

Tobias Becker,[1] Cedric Cappel,[2] Francesco Di Matteo,[3,4] Giovanna Sonsalla,[5,6,7] Ewelina Kaminska,[1] Fabio Spada,[1] Silvia Cappello,[3] Markus Damme,[2] and Pavel Kielkowski[1,8,*]

SUMMARY

Protein AMPylation is a posttranslational modification with an emerging role in neurodevelopment. In metazoans two highly conserved protein AMP-transferases together with a diverse group of AMPylated proteins have been identified using chemical proteomics and biochemical techniques. However, the function of AMPylation remains largely unknown. Particularly problematic is the localization of thus far identified AMPylated proteins and putative AMP-transferases. We show that protein AMPylation is likely a posttranslational modification of luminal lysosomal proteins characteristic in differentiating neurons. Through a combination of chemical proteomics, gel-based separation of modified and unmodified proteins, and an activity assay, we determine that the modified, lysosomal soluble form of exonuclease PLD3 increases dramatically during neuronal maturation and that AMPylation correlates with its catalytic activity. Together, our findings indicate that AMPylation is a so far unknown lysosomal posttranslational modification connected to neuronal differentiation and it may provide a molecular rationale behind lysosomal storage diseases and neurodegeneration.

INTRODUCTION

Protein posttranslational modifications (PTMs) provide the cell with mechanisms to swiftly react on internal and external clues to maintain the cellular homeostasis. Disruption of the protein homeostasis (proteostasis) is a hallmark of many neurodegenerative disorders (Hipp et al., 2019). Regulation of protein function by PTMs includes modulation of protein's catalytic activity, localization or protein-protein interactions (Aebersold et al., 2018). Protein AMPylation comprises the attachment of adenosine 5′-*O*-monophosphate (AMP) onto serine, threonine, and tyrosine amino acid side chains (Figure 1A) (Sieber et al., 2020). So far two AMP transferases are known in metazoans to catalyze protein AMPylation, protein adenylyltransferase FICD (FICD), and SelO (SELENOO) (Casey and Orth, 2017; Sreelatha et al., 2018). FICD is characterized by its endoplasmic reticulum (ER) localization and dual catalytical activity of AMPylation and deAMPylation (Preissler et al., 2017; Sengupta et al., 2019). FICD catalyzes an AMP transfer from its substrate ATP and reverses the modification by the hydrolysis of the AMP-protein ester. FICD's catalytic activity is regulated by its α-helix inhibition loop through the interaction of Glu234 positioned in the inhibition loop and Arg374, which is necessary for the complexation of ATP in the active site (Engel et al., 2012). Initial biochemical studies identified the ER localized heat shock protein HSPA5 (also called BiP or GRP78) as a cognate substrate of FICD (Ham et al., 2014; Sanyal et al., 2015). AMPylation of HSPA5 inhibits its chaperon activity and the downstream unfolded protein response cascade (Preissler et al., 2015). Furthermore, FICD's activity was recently shown to accelerate the neuronal differentiation of progenitor cells in human cerebral organoids, a tissue model of the human cerebral cortex (Kielkowski et al., 2020a). Surprisingly, apart from the increased number of neurons in tissue overexpressing FICD, some neurons displayed migratory defects. The neuronal role of the FIC domain was as well demonstrated in *Drosophila*, in which it is required for the visual neurotransmission in glial capitate projections (Rahman et al., 2012). In addition, FICD was shown to AMPylate α-synuclein *in vitro* (Sanyal et al., 2019). In *Caenorhabditis elegans* FICD has been reported to regulate the aggregation of amyloid-β and α-synuclein (Truttmann et al., 2018). In contrast, there are only scarce data about the function of SelO and its protein substrates (Sreelatha et al., 2018).

Several complementary strategies were introduced to analyze protein AMPylation, including isotopically labeled adenosine probes (Pieles et al., 2014), radioactively labeled adenosine nucleotides, antibodies (Kingdon et al., 1967; Yarbrough et al., 2009), microarrays (Yu and LaBaer, 2015), N^6-biotin-modified ATP

[1]LMU Munich, Department of Chemistry, Butenandtstr. 5-13, 81377 Munich, Germany

[2]University of Kiel, Institute of Biochemistry, Olshausenstr. 40, 24098 Kiel, Germany

[3]Max Planck Institute of Psychiatry, Kraepelinstraße 2, 80804 Munich, Germany

[4]International Max Planck Research School for Translational Psychiatry (IMPRS-TP), Kraepelinstraße 2-10, 80804 Munich, Germany

[5]LMU Munich, Department of Physiological Genomics, Biomedical Center (BMC), Großhadernerstr. 9, 82152 Planegg, Germany

[6]Helmholtz Zentrum München, Institute for Stem Cell Research, Ingolstädter Landstr. 1, 85764 Neuherberg, Germany

[7]Graduate School of Systemic Neurosciences (GSN), Großhadernerstr. 2, 82152 Planegg, Germany

[8]Lead contact

*Correspondence: pavel.kielkowski@cup.lmu.de

https://doi.org/10.1016/j.isci.2021.103521

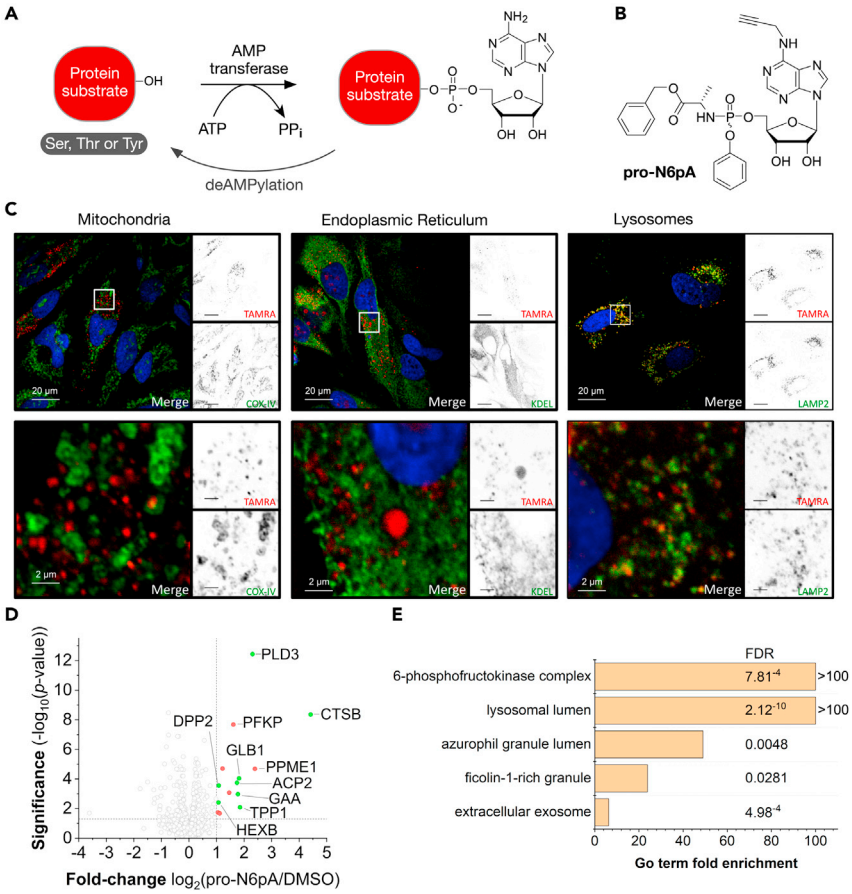

Figure 1. Human neuroblastoma cells (SH-SY5Y) display an enrichment of pro-N6pA probe-labeled proteins in lysosomes

(A) Schematic representation of protein AMPylation.

(B) Structure of the pro-N6pA probe for *in situ* labeling of potentially AMPylated proteins.

(C) Click chemistry staining of pro-N6pA with TAMRA-N_3 (red) and immunocytochemical staining in SH-SY5Y and colocalizations with markers for lysosome (LAMP2), ER (KDEL), and mitochondria (COX-IV).

(D) Volcano plot showing the significantly enriched AMPylated proteins from SH-SY5Y cells. Proteins localized to lysosome are depicted in green. Significantly enriched protein hits with other subcellular localization are in red (cutoff lines at 2-fold enrichment and *p* value of 0.05).

(E) GO terms analysis of significantly enriched proteins in SH-SY5Y cells.

(Sreelatha et al., 2018), and N^6-propargyl adenosine 5′-*O*-triphosphate (N6pATP) or phosphoramidate (Broncel et al., 2012; Grammel et al., 2011; Kielkowski et al., 2020a, 2020b). We have recently developed a chemical proteomic approach that allows high-throughput screening of protein AMPylation and comparison of the AMPylation levels between different conditions. This strategy utilizes the N^6-propargyl or N^6-ethylazide adenosine phosphoramidate (pro-N6pA and pro-N6azA, respectively) probes, which are metabolically activated to the corresponding N^6-modified adenosine triphosphate upon uptake into cells and used by endogenous AMP-transferases or by bacterial effectors in infection studies for protein AMPylation (Figure 1B) (Kielkowski et al., 2020a, 2020b; Rauh et al., 2020). Of note, the resulting N^6-modified ATP is inherently in competition with endogenous ATP and thus cannot report on the exact stoichiometry of protein AMPylation. The application of this chemical proteomic strategy in various cell types has revealed that protein AMPylation is more prevalent than previously assumed. Interestingly, it has led to the identification of a large group of protein substrates from different subcellular compartments that are not restricted to the ER, including cytosolic (PFKP, SQSTM1), nucleolar (PPME1), cytoskeletal (TUBB, MAP2), and lysosomal (CTSB, PLD3, and ACP2) proteins (Broncel et al., 2016; Kielkowski et al., 2020a). In particular, in the lysosome, there is only limited evidence on PTMs of luminal lysosomal proteins other than N-glycosylation amid numerous diseases associated with lysosomal proteins such as the lysosomal acid phosphatase

ACP2 in lysosomal storage diseases (LSDs) or the 5′-3′ exonuclease PLD3 in Alzheimer's disease and autoinflammatory diseases (Cappel et al., 2021; Cruchaga et al., 2014; Gavin et al., 2021; Gonzalez et al., 2018; Marques and Saftig, 2019; Schultz et al., 2011; Stadlmann et al., 2017; Stoka et al., 2016). Therefore, the discovery of lysosomal protein PTMs might shed new light on the regulation of their function, localization, and protein-protein interactions and hence putatively uncover unknown pathophysiologic mechanisms.

Here, we characterize protein AMPylation during neuronal differentiation and maturation by a combination of chemical proteomics and a gel-based approach. Thereby, we provide supporting evidence that the two lysosomal proteins PLD3 and ACP2 are increasingly AMPylated during neural differentiation and that the AMPylation of PLD3 correlates with the inhibition of its catalytic activity.

RESULTS

AMPylated proteins localize to lysosomes in SH-SY5Y neuroblastoma cells

We have developed a chemical proteomic strategy in previous studies to analyze the protein AMPylation in living cells using the cell-permeable pro-N6pA probe (Kielkowski et al., 2020a, 2020b). In this study, we have started with the completion of this dataset using fluorescence imaging of the SH-SY5Y cells treated with the pro-N6pA probe to visualize the subcellular localization of potentially AMPylated proteins. Interestingly, probe-labeled proteins exhibit a vesicular distribution pattern overlapping with lysosomes as confirmed by co-staining with the lysosomal-specific marker LAMP2 (Figure 1C). Colocalization of the majority of pro-N6pA probe signal with the ER and mitochondria was excluded by co-staining of the pro-N6pA probe with antibodies against KDEL and COX-IV, respectively. These findings point to an enrichment of AMPylated proteins in lysosomes and raise questions about the localization and origin of their AMPylation. GO analysis of chemical proteomics data from SH-SY5Y cells indicated an overrepresentation of lysosomal proteins among those enriched for AMPylation by 54% of all significantly enriched proteins. These include CTSB, PLD3, GAA, GLB1, TPP1, HEXB, DPP2, and GUSB, with PLD3 and CTSB showing the strongest enrichment (Figures 1D and 1E). Next, we asked whether AMPylation of lysosomal proteins changes during neuronal differentiation and maturation and how the AMPylation status correlates with non-neuronal cell types. Although the chemical proteomic analysis of protein AMPylation variation during neuronal differentiation was previously performed, it has focused solely on two differentiation stages, neuronal progenitors (NPCs) and mature neurons. To investigate the AMPylation of lysosomal proteins in differentiating neurons with higher temporal resolution, we searched for a suitable cellular system that would allow collecting sufficient amounts of total proteins for chemical proteomic analysis in shorter periods of time and thus overcoming the bottlenecks of the standard human induced pluripotent stem cells (iPSCs) differentiation protocols (Boyer et al., 2012).

Chemical proteomic analysis of protein AMPylation in differentiating iNGN cells

To map the changes in protein AMPylation during the neuronal differentiation in more detail, we took advantage of the human induced pluripotent stem cells with inducible overexpression of a pair of transcription factors, Neurogenin-1 and Neurogenin-2, leading to their rapid differentiation into a homogeneous population of functional bipolar neurons within 4 days (iNGN) (Busskamp et al., 2014). The changes in AMPylation were followed at six time points during the iNGN differentiation and maturation using the previously described chemical proteomics strategy utilizing a metabolically activated pro-N6pA probe (Figure 2A). In brief, cells were treated with the pro-N6pA probe 16 h prior to their harvest to allow metabolic activation to the corresponding N^6-propargyl ATP, which is used as a substrate by endogenous AMP-transferases to label proteins. Subsequently, the cells were lysed and the alkyne modified proteins were further coupled with biotin-PEG-azide by Cu(I) catalyzed click chemistry. The pro-N6pA labeled and biotinylated proteins were then enriched on avidin-coated agarose beads and on beads trypsinized to yield complex peptide mixtures, which were resolved by LC-MS/MS measurements. The resulting label-free quantification (LFQ) of proteins from four replicates and their comparison with DMSO-treated cells prepared in the same manner provided the quantitative differences in protein AMPylations between undifferentiated and differentiated iNGN cells (Figures 2B and S1, Tables S1, S2, S3, S4, S5, S6, and S8). Of note, owing to the metabolic activation of the pro-N6pA probe, a minor incorporation, for example, as ADP-ribosylation, cannot be completely excluded. The background from unspecific protein binding to the avidin-agarose beads in both vehicle control (DMSO) and probe-treated cells partially reflects the total protein expression level. To correct for this contribution, we have carried out the whole proteome analysis of iNGNs during the course of differentiation (Figure S2). In addition, the whole proteome analysis confirmed the identity of the cells and the progress of neuronal differentiation and maturation (Figure S3 and Tables

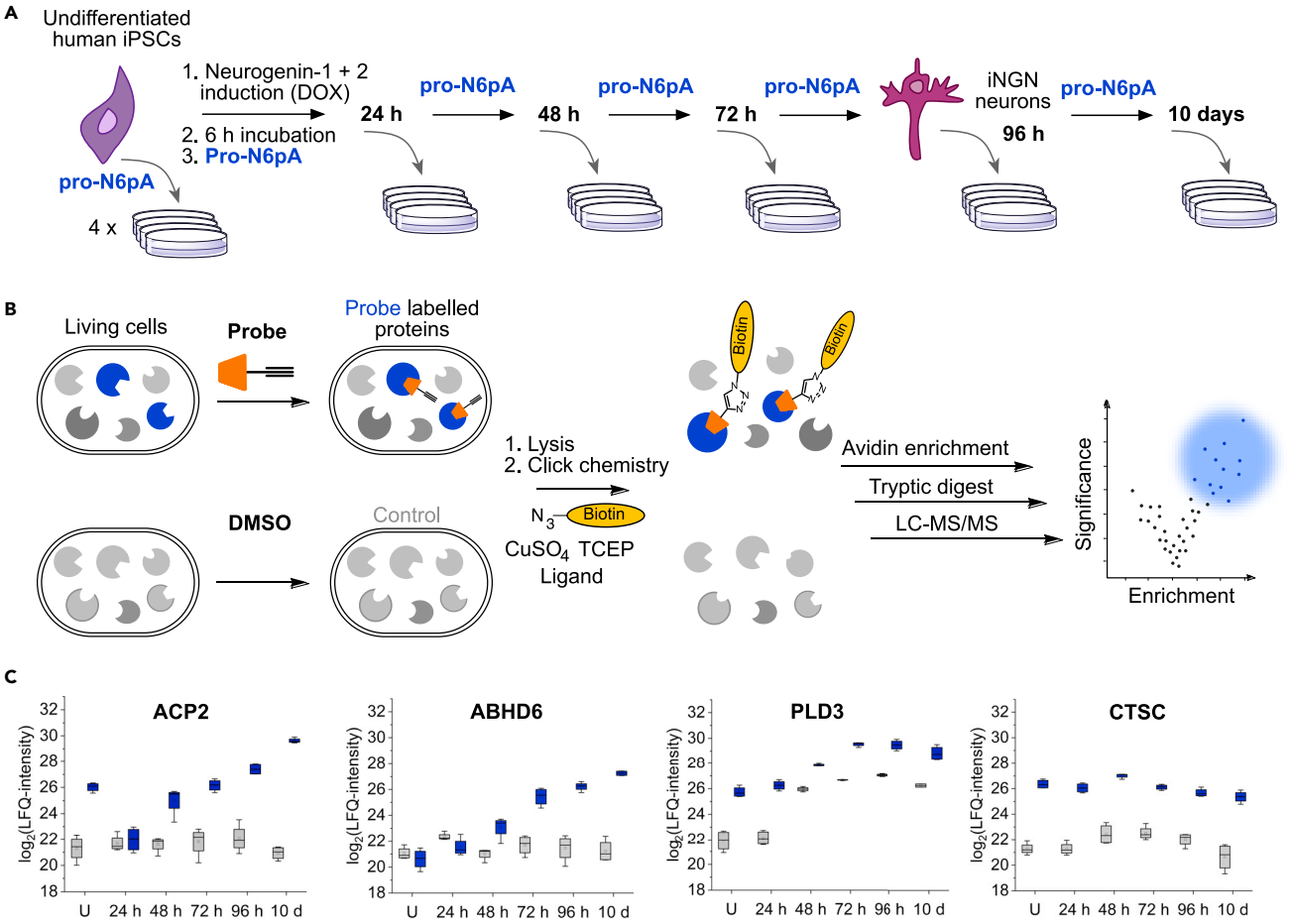

Figure 2. Chemical proteomics of neuronal differentiation and maturation shows specific patterns of protein AMPylation

(A) Schematic iNGNs differentiation procedure and pro-N6pA probe treatment.

(B) Chemical proteomic protocol comparing the probe and DMSO control-treated cells.

(C) Profile plots of significantly enriched proteins ACP2, ABHD6, PLD3, and CTSC from pro-N6pA probe-treated iNGNs. Blue boxes represent the LFQ-intensities from pro-N6pA probe-treated cells after enrichment. Gray boxes represent LFQ-intensities from control (DMSO-treated) cells, showing unspecific binding to avidin-coated agarose beads ($n = 4$, the box is defined by 25th and 75th percentile, whiskers show outliers, line is a median, and circle is a mean).

S7 and S8). The examination of the profile plots of the enriched proteins shows a distinct pattern of AMPylation dynamics during neuronal maturation (Figure 2C). The most distinct composition was observed for the two lysosomal proteins ACP2 and ABHD6, with a linear increase of probe incorporation during the course of differentiation, while the total expression level of both proteins remains stable during the process (Figures 2C and S2). On the other hand, other lysosomal significantly enriched proteins show a stable AMPylation level, for example, CTSC. A similar increase during iNGNs differentiation was observed for the cytosolic protein ATP-dependent 6-phosphofructokinase PFKP, a gatekeeper of glycolysis (Figure S2). Next, we focused on the lysosomal protein PLD3, which was recently associated with Alzheimer's disease, but its physiological function in neurons and regulation have been so far controversial (Arranz et al., 2017; Cruchaga et al., 2014). As shown previously, whole proteome analysis of PLD3 exhibits an increase of PLD3 in neurons compared with undifferentiated iNGNs. PLD3 is known to be transported from the ER and Golgi via endosomes to lysosomes, where the cytosolic N-terminal membrane-bound domain of full-length PLD3 is proteolytically cleaved. The resulting soluble luminal PLD3 containing the putative active site is delivered to the lysosomes (Gonzalez et al., 2018). Both chemical proteomics and whole proteome analysis cannot provide the information on which form of PLD3 is likely to be modified by AMPylation. Thus, we focused on the development of a gel-based methodology that would allow the separation of different protein forms as well as the quantification of the protein AMPylation levels. Previously, isoelectric focusing gels have been

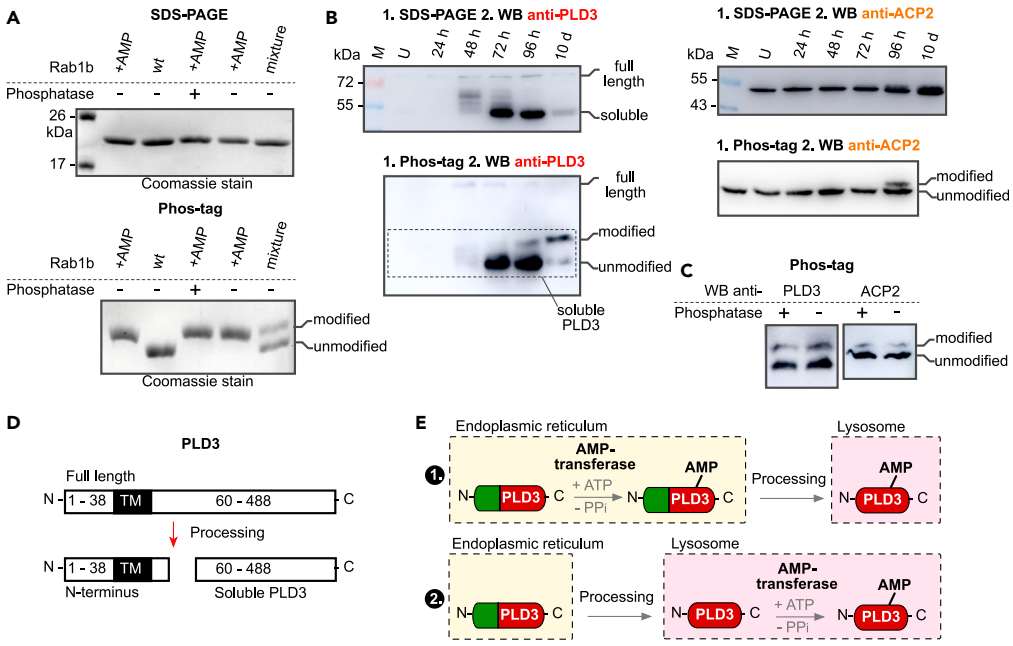

Figure 3. Phos-tag ligand SDS-PAGE distinguishes unmodified and AMPylated proteins

(A) Coomassie-stained SDS-PAGE and Phos-tag ligand containing SDS-PAGE gel separation of unmodified (wt) and AMPylated (+AMP) recombinant Rab1b. With and without treatment with the shrimp alkaline phosphatase (±).

(B) PLD3 and ACP2 Phos-tag ligand SDS-PAGE separation and western blotting during iNGNs differentiation and maturation. Visualization using the anti-PLD3 and anti-ACP2 antibodies.

(C) Phos-tag SDS-PAGE analysis of the PLD3 and ACP2 PTM status after phosphatase treatment.

(D) Processing of the full-length PLD3 into soluble active PLD3.

(E) Scheme showing the two different scenarios of putative intracellular trafficking and AMPylation of the PLD3. M stands for protein marker.

used for the separation of AMPylated HSPA5 from its unmodified form, but the separation of the two species appears to be rather limited (Preissler et al., 2015). Therefore, we explored the possibility to use another gel-based method, which also takes advantage of the presence of a phosphate moiety, but utilize the Phos-tag ligand (Kinoshita et al., 2004, 2006).

Phos-tag ligand-based polyacrylamide gel electrophoresis separates the modified and unmodified proteins

In order to validate our results from chemical proteomics experiments by a complementary method, which would not rely on the pro-N6pA probe and mass spectrometry, we have concentrated on the development of a gel-based approach. Therefore, we have tested the possibility to capture the monophosphate moiety of AMPylated proteins using an alkoxide-bridge Mn^{2+} metal complex bound in the gel by Phos-tag ligand. We have used a recombinant Rab1b protein, which was AMPylated *in vitro* by the recombinant bacterial effector DrrA (Du et al., 2021). The Rab1b identities were confirmed by top-down mass spectrometry (Figure S4). To prepare a Phos-Tag gel, conventional sodium dodecyl sulfate (SDS)-polyacrylamide gels (SDS-PAGEs) were supplemented with the commercially available Mn^{2+} ion-binding Phos-tag ligand. Direct comparison of non-AMPylated, AMPylated, and 1:1 mixture of both modified and unmodified Rab1b showed that indeed the Phos-tag ligand added to standard SDS-PAGE resolves the two species and yields two clearly separated bands as visualized by Coomassie staining (Figure 3A). A control experiment using SDS-PAGE without addition of the Phos-tag ligand showed no separation of the two species (Figure 3A). Because the Phos-tag ligand was initially developed for separation of the phosphorylated proteins, we have treated the *in vitro* AMPylated Rab1b with shrimp alkaline phosphatase to exclude the potential separation due to protein phosphorylation and to show the resistance of the AMP moiety against the phosphatase cleavage (Figure 3A). The activity of the phosphatase was verified by hydrolysis of the phosphorylated ovalbumin (Figure S5). Next, we examined whether it is possible to separate AMPylated HSPA5 from its

unmodified form in HeLa cell lysates. Therefore, after separation the Phos-Tag gel was blotted onto a PVDF membrane and visualized by staining with an anti-HSPA5 antibody. We observed a clear separation of the two forms, confirming our hypothesis that the Phos-tag ligand can be used for the separation of the AMPylated proteins in lysates (Figure S6). Hence, we have established the Phos-tag ligand-functionalized SDS-PAGE separation as a useful method for analysis of AMPylated proteins, which overcomes the necessity for treatment with the probe, and thus it can be used for analysis of protein AMPylation from a wider range of sources, for example, from animal tissues. In our chemical proteomics experiment, we have identified several AMPylated lysosomal proteins, including PLD3 and ACP2. PLD3 can exist either as the full-length protein or as the active soluble form localized in lysosomes, which is obtained by cleavage of the N terminus containing the transmembrane domain (Figure 3D) (Gonzalez et al., 2018). To obtain better insight into the changes of full-length, soluble, and modified PLD3 during neuronal differentiation, we performed the Phos-tag gel-based separation from undifferentiated iNGNs, and iNGNs differentiated between 1 and 10 days. To our surprise, we observed the modified soluble form of PLD3 only after 4 days of differentiation, with a majority of modified PLD3 in 10-day differentiated neurons, which is in line with our observation of increasing pro-N6pA labeling of PLD3 from the chemical proteomics study (Figures 3B and S7). Moreover, analysis by standard SDS-PAGE showed that the soluble lysosomal PLD3 form increases dramatically with increasing time of iNGN differentiation (up to 72 h), whereas it drops substantially upon maturation of iNGN neurons between 4 and 10 days post induction (Figure 3B). In addition to PLD3, a similar AMPylation trend was observed for another lysosomal protein, ACP2, further corroborating the chemical proteomic results and pointing to a specific function of probable protein AMPylation in neuronal maturation (Figure 3B) (Makrypidi et al., 2012). To exclude the separation due to the protein phosphorylation, lysates from the 10-day differentiated iNGNs were treated with the shrimp alkaline phosphatase (Figure 3C). Taken together, the combination of standard SDS-PAGE and Phos-tag-based gel electrophoresis enabled a detailed characterization of PLD3 post-translational processing and AMPylation dynamics during neuronal differentiation and maturation. More specifically, the amount of active soluble PLD3 increases during the differentiation process (up to 72), whereas its AMPylation raises during maturation of iNGN neurons (96 h–10 d). However, the identity and localization of the AMP transferase catalyzing the PLD3 AMPylation remains unknown, thus leaving two plausible scenarios of its AMPylation processing and trafficking into lysosomes (Figure 3E). Even though both methods correlate and point that the observed modification is indeed AMPylation, the exact identity of the PTM has not been confirmed by a direct mass spectrometry experiment. We have attempted to identify the AMPylation site of PLD3. For this, we enriched PLD3 by immunoprecipitation before digestion with trypsin and LC-MS/MS analysis. However, perhaps due to the low sequence coverage (53%) it did not lead to identification of the modification site. In order to specifically enrich only the modified peptides from lysates, we performed enrichment using the desthiobiotin linker, which allows one to selectively elute modified peptides after the enrichment and tryptic digestion (Zanon et al., 2020). Unfortunately, spectra analysis did not lead to identification of either PLD3 or any other site including T518 on the HSPA5. This is likely caused by the low ionization efficiency, fragmentation of the adenosine, and the low abundance of AMPylated peptides.

PTM status correlates with the PLD3 activity in iNGN neurons

To correlate the catalytic activity of PLD3 with its PTM status during the course of iNGNs differentiation, a PLD3-specific acid 5′ exonuclease activity assay was carried out (Cappel et al., 2021). Therefore, whole-cell lysates of iNGN cells were incubated with a fluorophore- and quencher-coupled oligodesoxynucleotide. A 5′ exonucleolytic digest thereby led to a proportional increase in fluorescence signal, measured kinetically over 12 h. The overall activity of PLD3 per total cellular protein increases during the differentiation, which can be accounted for by the increasing levels of its soluble form in lysosomes. In contrast, the PLD3 activity decreases significantly from the 4th day to the 10th day after induction of the differentiation, coinciding with increasing AMPylation of the soluble form during neuronal maturation (Figure 4A). This observation suggests that AMPylation might inhibit PLD3's catalytic activity, which is in line with previous reports on inhibition of the chaperon activity of HSPA5 and the peptidase activity of CTSB.

Directed differentiation of physiological human iPSCs shows the modified PLD3 as the only soluble form in young and mature neurons

In order to compare the AMPylation pattern obtained from the highly homogeneous and robust differentiation and maturation of iNGN cells we have collected lysates from physiological iPSCs, young and mature neurons differentiated for 5 and 10 weeks, respectively (Figures 4B and S8) (Gunhanlar et al., 2018). The modified, likely AMPylated soluble form was the only PLD3 species detectable by Phos-tag SDS-PAGE

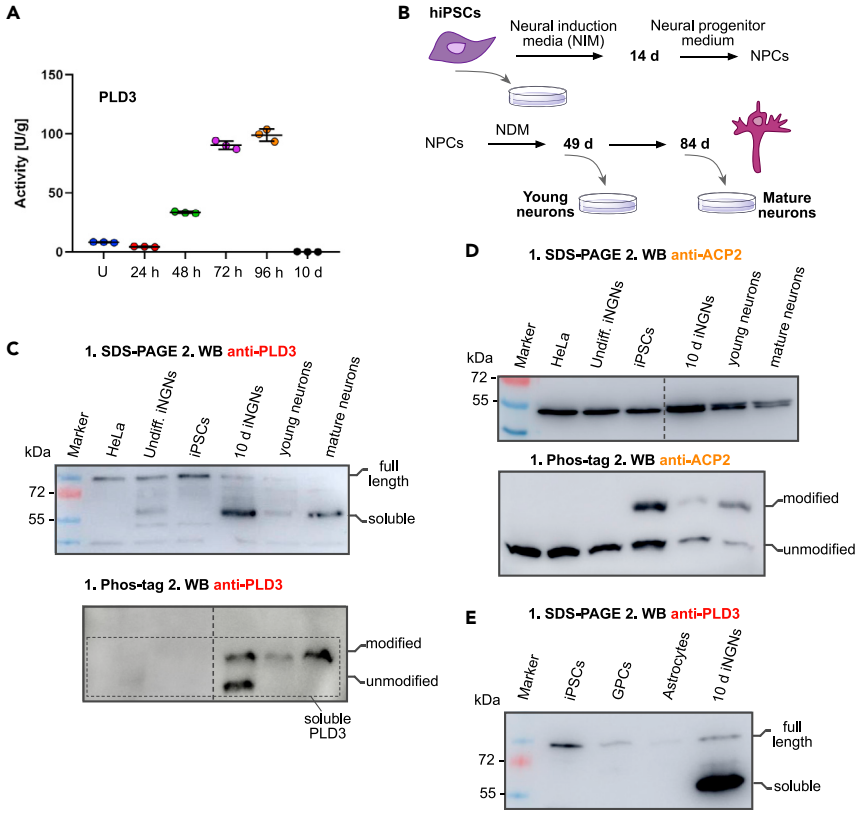

Figure 4. Modification of PLD3 correlates with its activity in neurons

(A) PLD3 5′ exonuclease activity assay correlates the amount of the soluble PLD3 form with its activity and shows the modification to inhibit the catalytic activity (n = 3, line indicates the mean, error bars show the standard deviation).

(B) Directed differentiation protocol of human iPSCs into dopaminergic neurons. NDM, neural differentiation medium.

(C) SDS-PAGE and Phos-tag ligand SDS-PAGE separations followed by western blot using the anti-PLD3 antibody show pronounced and nearly quantitative modification, likely AMPylation of PLD3 in dopaminergic neurons compared with the iNGN forward reprogramming.

(D) ACP2 SDS-PAGE and Phos-tag ligand SDS-PAGE separations followed by western blot using anti-ACP2 antibody.

(E) SDS-PAGE followed by western blot using the anti-PLD3 antibody detects solely the full-length PLD3 in iPSCs, GPCs, and astrocytes.

in young as well as in mature neurons, whereas in undifferentiated iPSCs the anti-PLD3 antibody detected no soluble form, whether unmodified or modified (Figures 4C and S9). Comparison of the PLD3 pattern in 10-day differentiated iNGNs, young and mature physiological neurons, with that in lysates from HeLa cells and undifferentiated iPSCs and iNGNs shows that the soluble forms, whether unmodified or AMPylated, are specific to neurons. Moreover, the analysis of PLD3 processing and AMPylation during differentiation of iPSCs into glial progenitor cells (GPCs) and astrocytes confirmed the specificity of this process for the neuronal cell lineage (Figure 4E, see Figure S9 for Phos-tag SDS-PAGE analysis). A similar degree of ACP2 modification was seen in 10-day differentiated iNGN and physiologically mature neural networks (Figure 4D). Taken together, these findings further corroborate the hypothesis that AMPylation plays a specific role in maturation of human neurons.

DISCUSSION

Lysosomal dysfunction is linked to several human pathologies such as LSDs, cancer, neurodegeneration, and aging (Marques and Saftig, 2019). Neuronal cells are particularly sensitive to impaired lysosomal function owing to their tightly controlled differentiation process and postmitotic character. Even though the genetic basis and the biochemistry underlying these diseases are known, the cellular and molecular mechanisms leading to disruption of neuronal viability remain to be understood. Our study describes lysosomal

proteins to be significantly enriched among the AMPylated proteins with changing stoichiometry at various stages of neuronal differentiation, pointing to a specific function of protein AMPylation during differentiation and maturation. The fine-tuning of the lysosomal activity was recently reported to be critical for maintenance of the quiescent neural stem cells fitness and their activation responsiveness (Leeman et al., 2018). Thus, the precise orchestration of these processes might be achieved by adding an extra regulatory layer of protein PTMs, including AMPylation. Furthermore, comparison of the expression levels of the identified AMPylated proteins during the development of mouse and human embryos as well as human organoids shows clear differences between the species and model systems pointing to a regulation of the proteins at different levels and stages of gestation (Figure S10) (Klingler et al., 2021). The gel-based analyses of PLD3 showed a striking increase of the modified soluble form in differentiated iNGN neurons. Comparing the iNGN forward reprogramming model of neuronal differentiation with differentiation of physiological human iPSCs into young and mature neurons showed an even stronger trend with fully modified PLD3 in mature physiological neurons. Prolonging the neurogenic period gives rise to more neurons and expansion of the upper layer of neocortex (Stepien et al., 2020). Thus, lengthening the maturation period of the physiological neurons in comparison with the fast differentiation of iNGN cells may provide more time to establish a more strictly defined modification status of PLD3. In particular, the increased expression of PLD3 was shown to coincide with late neuronal development in the hippocampus and the primary somatosensory cortex (Pedersen et al., 1998). In consequence, the PLD3 AMPylation may modulate PLD3 activity or stability to ensure the proper lysosomal function during the migration and maturation of the basal progenitors from the cortical subventricular zone. The activity assay of PLD3 revealed that the probable AMPylation status correlates with its activity in iNGN neurons. Even though we have characterized the progress of the PLD3 AMPylation in detail, it remains to be elucidated where the AMPylation of PLD3 occurs and which AMP-transferase catalyzes the attachment of this modification (Figure 3E) or if it can be reversed by active deAMPylation. The heterogeneity of the cell types in the human cortex is enormous, including excitatory and inhibitory neurons, astrocytes, microglia, and oligodendrocytes. Analysis of the expression levels of the lysosomal proteins ACP2, ABHD6, PLD3, and CTSC in these cell types exhibits substantial differences (Figure S11) (Kanton et al., 2019). Together with considerable variance in the PTM status, as we have demonstrated for PLD3 in astrocytes and neuronal cell lineage, it highlights the diversity and specificity of the proteoforms in the central nervous system. Therefore, in future studies, it will be important to compare the AMPylation status of these proteins in different cell types and to elucidate the functional consequences. Our study provides evidence that AMPylation is likely a rare modification of the lysosomal proteins and thus gives insight into a putative mechanism modulating the protein activity in this critical cellular department. This finding may open up new possibilities for designing therapeutic strategies against the damage linked to lysosomal dysfunction during neurodevelopment, cancer, and aging.

Limitations of the study

The combination of the two methods, MS-based chemical proteomics and Phos-tag ligand gel analysis, strongly supports the AMPylation of several lysosomal proteins; however, a direct proof for AMPylation is missing in this study. The main bottleneck in using mass spectrometry for validation is the inherent instability of the adenosine monophosphate moiety and the low abundance of the modified peptides. In cells, the pro-N6pA probe is converted to the corresponding N^6-propargyl ATP, which might be further metabolized to N^6-propargyl NAD^+ and incorporated onto proteins as ADP-ribosylation. Although we have shown in our previous study (Kielkowski et al., 2020a) that the amounts are negligible, it cannot be excluded under different experimental conditions. Together, the protein PTM status of lysosomal proteins observed in the chemical proteomic experiments correlates well with the Phos-tag ligand SDS-PAGE analysis. Nevertheless, the limitation of the Phos-tag gel separation is that it cannot distinguish between different NMPylations such as UMPylation or GMPylation. Further development of mass spectrometry experiments should determine the identity of the PTM.

STAR★METHODS

Detailed methods are provided in the online version of this paper and include the following:

- KEY RESOURCES TABLE
- RESOURCE AVAILABILITY
  - Lead contact
  - Materials availability
  - Data and code availability

SUPPLEMENTAL INFORMATION

Supplemental information can be found online at https://doi.org/10.1016/j.isci.2021.103521.

ACKNOWLEDGMENTS

This research was supported by the Liebig fellowship from Fund of the association of the chemical industry (VCI) to P.K. and T.B., LMUexcellent Junior Fund to P.K., and Deutsche Forschungsgemeinschaft (DFG, German Research Foundation) – SFB 1309. We are grateful for the kind gift of recombinant Rab1b wt and AMPylated form from the group of Dr. Sabine Schneider by Dr. Marie-Kristin von Wrisberg.

AUTHOR CONTRIBUTIONS

P.K., M.D., and T.B. conceived the study. T.B. cultured and differentiated the iNGN cells. T.B. carried out all proteomic experiments and gel-based analyses. C.C. performed the fluorescence imaging and PLD3 activity assay. F.D.M. cultured the physiological hiPSCs and differentiated them into neurons. G.S. cultured the hiPSCs and differentiated them into GPCs and astrocytes. E.K. and F.S. helped to establish the iNGN cell culture and reviewed the manuscript. P.K. and T.B. wrote the manuscript. All authors revised the manuscript.

DECLARATION OF INTERESTS

The authors declare no competing interests.

Received: March 10, 2021
Revised: July 20, 2021
Accepted: November 23, 2021
Published: December 17, 2021

REFERENCES

Aebersold, R., Agar, J.N., Amster, I.J., Baker, M.S., Bertozzi, C.R., Boja, E.S., Costello, C.E., Cravatt, B.F., Fenselau, C., Garcia, B.A., et al. (2018). How many human proteoforms are there? Nat. Chem. Biol. *14*, 206–214.

Arranz, A.M., Strooper, B., Frigerio, C., Horre, K., Fazzari, P., Saido, T.C., and Saito, T. (2017). PLD3 gene and processing of APP. Nature *541*, E1.

Ayo-Martin, A.C., Kyrousi, C., Giaimo, R.D., and Cappello, S. (2020). GNG5 controls the number of apical and basal progenitors and alters neuronal migration during cortical development. Front. Mol. Biosci. *7*, 578137.

Biedler, J.L., Helson, L., and Spengler, B.A. (1973). Morphology and growth, tumorigenicity, and cytogenetics of human neuroblastoma cells in continuous culture. Cancer Res. *33*, 2643–2652.

Boyer, L.F., Campbell, B., Larkin, S., Mu, Y., and Gage, F.H. (2012). Current Protocols in Stem Cell Biology (Wiley), pp. 1H.6.1–1H.6.11.

Broncel, M., Serwa, R.A., and Tate, E.W. (2012). A new chemical handle for protein AMPylation at the host–pathogen interface. ChemBioChem *13*, 183–185.

Broncel, M., Serwa, R.A., Bunney, T.D., Katan, M., and Tate, E.W. (2016). Global profiling of huntingtin-associated protein E (HYPE)-Mediated AMPylation through a chemical proteomic approach. Mol. Cell Proteomics *15*, 715–725.

Busskamp, V., Lewis, N.E., Guye, P., Ng, A.H., Shipman, S.L., Byrne, S.M., Sanjana, N.E., Murn, J., Li, Y., Li, S., et al. (2014). Rapid neurogenesis through transcriptional activation in human stem cells. Mol. Syst. Biol. *10*, 760.

Cappel, C., Gonzalez, A.C., and Damme, M. (2021). Quantification and characterization of the 5′ exonuclease activity of the lysosomal nuclease PLD3 by a novel cell-based assay. J. Biol. Chem. *296*, 100152.

Casey, A.K., and Orth, K. (2017). Enzymes involved in AMPylation and deAMPylation. Chem. Rev. *118*, 1199–1215.

Cox, J., Hein, M.Y., Luber, C.A., Paron, I., Nagaraj, N., and Mann, M. (2014). Accurate proteome-wide label-free quantification by delayed normalization and maximal peptide ratio extraction, termed MaxLFQ. Mol. Cell Proteomics *13*, 2513–2526.

Cruchaga, C., Karch, C.M., Jin, S., Benitez, B.A., Cai, Y., Guerreiro, R., Harari, O., Norton, J., Budde, J., Bertelsen, S., et al. (2014). Rare coding variants in the phospholipase D3 gene confer risk for Alzheimer's disease. Nature *505*, 550.

Du, J., Wrisberg, M.-K., Gulen, B., Stahl, M., Pett, C., Hedberg, C., Lang, K., Schneider, S., and Itzen, A. (2021). Rab1-AMPylation by Legionella DrrA is allosterically activated by Rab1. Nat. Commun. *12*, 460.

Engel, P., Goepfert, A., Stanger, F.V., Harms, A., Schmidt, A., Schirmer, T., and Dehio, C. (2012). Adenylylation control by intra- or intermolecular active-site obstruction in Fic proteins. Nature *482*, 107–110.

Gavin, A.L., Huang, D., Blane, T.R., Thinnes, T.C., Murakami, Y., Fukui, R., Miyake, K., and Nemazee, D. (2021). Cleavage of DNA and RNA by PLD3 and PLD4 limits autoinflammatory triggering by multiple sensors. Nat. Commun. *12*, 5874.

Gonzalez, A.C., Schweizer, M., Jagdmann, S., Bernreuther, C., Reinheckel, T., Saftig, P., and Damme, M. (2018). Unconventional trafficking of mammalian phospholipase D3 to lysosomes. Cell Rep. *22*, 1040–1053.

Grammel, M., Luong, P., Orth, K., and Hang, H.C. (2011). A chemical reporter for protein AMPylation. J. Am. Chem. Soc. *133*, 17103–17105.

Gunhanlar, N., Shpak, G., van der Kroeg, M., Gouty-Colomer, L.A., Munshi, S.T., Lendemeijer, B., Ghazvini, M., Dupont, C., Hoogendijk, W.J.G., Gribnau, J., et al. (2018). A simplified protocol for differentiation of electrophysiologically mature neuronal networks from human induced pluripotent stem cells. Mol. Psychiatr. *23*, 1336–1344.

Ham, H., Woolery, A.R., Tracy, C., Stenesen, D., Krämer, H., and Orth, K. (2014). Unfolded protein response-regulated Drosophila Fic (dFic) protein reversibly AMPylates BiP chaperone during endoplasmic reticulum homeostasis. J. Biol. Chem. *289*, 36059–36069.

Hipp, M.S., Kasturi, P., and Hartl, F.U. (2019). The proteostasis network and its decline in ageing. Nat. Rev. Mol. Cell Biol. *20*, 421–435.

Kanton, S., Boyle, M.J., He, Z., Santel, M., Weigert, A., Sanchís-Calleja, F., Guijarro, P., Sidow, L., Fleck, J.S., Han, D., et al. (2019). Organoid single-cell genomic atlas uncovers human-specific features of brain development. Nature *574*, 418–422.

Kielkowski, P., Buchsbaum, I.Y., Kirsch, V.C., Bach, N.C., Drukker, M., Cappello, S., and Sieber, S.A. (2020a). FICD activity and AMPylation remodelling modulate human neurogenesis. Nat. Commun. *11*, 517.

Kielkowski, P., Buchsbaum, I.Y., Becker, T., Bach, K., Cappello, S., and Sieber, S.A. (2020b). A pronucleotide probe for live-cell imaging of protein AMPylation. Chembiochem *21*, 1285–1287.

Kingdon, H., Shapiro, B., and Stadtman, E. (1967). Regulation of glutamine synthetase. 8. ATP: glutamine synthetase adenylyltransferase, an enzyme that catalyzes alterations in the regulatory properties of glutamine synthetase. Proc. Natl. Acad. Sci. U S A *58*, 1703–1710.

Kinoshita, E., Takahashi, M., Takeda, H., Shiro, M., and Koike, T. (2004). Recognition of phosphate monoester dianion by an alkoxide-bridged dinuclear zinc(ii) complex. Dalton Trans *21*, 1189–1193.

Kinoshita, E., Kinoshita-Kikuta, E., Takiyama, K., and Koike, T. (2006). Phosphate-binding tag, a new tool to visualize phosphorylated proteins. Mol. Cell Proteomics *5*, 749–757.

Klaus, J., Kanton, S., Kyrousi, C., Ayo-Martin, A.C., Giaimo, R.D., Riesenberg, S., O'Neill, A.C., Camp, J.G., Tocco, C., Santel, M., et al. (2019). Altered neuronal migratory trajectories in human cerebral organoids derived from individuals with neuronal heterotopia. Nat. Med. *25*, 561–568.

Klingler, E., Francis, F., Jabaudon, D., and Cappello, S. (2021). Mapping the molecular and cellular complexity of cortical malformations. Science *371*, eaba4517.

Leeman, D.S., Hebestreit, K., Ruetz, T., Webb, A.E., McKay, A., Pollina, E.A., Dulken, B.W., Zhao, X., Yeo, R.W., Ho, T.T., et al. (2018). Lysosome activation clears aggregates and enhances quiescent neural stem cell activation during aging. Science *359*, 1277–1283.

Makrypidi, G., Damme, M., Müller-Loennies, S., Trusch, M., Schmidt, B., Schlüter, H., Heeren, J., Lübke, T., Saftig, P., and Braulke, T. (2012). Mannose 6 dephosphorylation of lysosomal proteins mediated by acid phosphatases Acp2 and Acp5. Mol. Cell Biol. *32*, 774–782.

Marques, A.R.A., and Saftig, P. (2019). Lysosomal storage disorders – challenges, concepts and avenues for therapy: beyond rare diseases. J. Cell Sci. *132*, jcs221739.

Pedersen, K.M., Finsen, B., Celis, J.E., and Jensen, N.A. (1998). Expression of a novel murine phospholipase D homolog coincides with late neuronal development in the forebrain. J. Biol. Chem. *273*, 31494–31504.

Pieles, K., Glatter, T., Harms, A., Schmidt, A., and Dehio, C. (2014). An experimental strategy for the identification of AMPylation targets from complex protein samples. Proteomics *14*, 1048–1052.

Preissler, S., Rato, C., Chen, R., Antrobus, R., Ding, S., Fearnley, I.M., and Ron, D. (2015). AMPylation matches BiP activity to client protein load in the endoplasmic reticulum. ELife *4*, e12621.

Preissler, S., Rato, C., Perera, L., Saudek, V., and Ron, D. (2017). FICD acts bifunctionally to AMPylate and de-AMPylate the endoplasmic reticulum chaperone BiP. Nat. Struct. Mol. Biol. *24*, 23–29.

Puck, T.T., and Marcus, P.I. (1955). A rapid method for viable cell titration and clone production with Hela cells in tissue culture: the use of X-irradiated cells to supply conditioning factors. Proc. Natl. Acad. Sci. U S A *41*, 432–437.

Rahman, M., Ham, H., Liu, X., Sugiura, Y., Orth, K., and Krämer, H. (2012). Visual neurotransmission in Drosophila requires expression of Fic in glial capitate projections. Nat. Neurosci. *15*, 871–875.

Rauh, T., Brameyer, S., Kielkowski, P., Jung, K., and Sieber, S.A. (2020). MS-based in situ proteomics reveals AMPylation of host proteins during bacterial infection. Acs Infect Dis. *6*, 3277–3289.

Santos, R., Vadodaria, K.C., Jaeger, B.N., Mei, A., Lefcochilos-Fogelquist, S., Mendes, A., Erikson, G., Shokhirev, M., Randolph-Moore, L., Fredlender, C., et al. (2017). Differentiation of inflammation-responsive astrocytes from glial progenitors generated from human induced pluripotent stem cells. Stem Cell Rep. *8*, 1757–1769.

Sanyal, A., Chen, A.J., Nakayasu, E.S., Lazar, C.S., Zbornik, E.A., Worby, C.A., Koller, A., and Mattoo, S. (2015). A novel link between fic (filamentation induced by cAMP)-mediated adenylylation/AMPylation and the unfolded protein response. J. Biol. Chem. *290*, 8482–8499.

Sanyal, A., Dutta, S., Camara, A., Chandran, A., Koller, A., Watson, B.G., Sengupta, R., Ysselstein, D., Montenegro, P., Cannon, J., et al. (2019). Alpha-synuclein is a target of fic-mediated adenylylation/AMPylation: possible implications for Parkinson's disease. J. Mol. Biol. *431*, 2266–2282.

Schultz, M.L., Tecedor, L., Chang, M., and Davidson, B.L. (2011). Clarifying lysosomal storage diseases. Trends Neurosci. *34*, 401–410.

Sengupta, R., Poderycki, M.J., and Mattoo, S. (2019). CryoAPEX - an electron tomography tool for subcellular localization of membrane proteins. J. Cell Sci. *132*, jcs222315.

Sieber, S.A., Cappello, S., and Kielkowski, P. (2020). From young to old: AMPylation hits the brain. Cell Chem. Biol. *27*, 773–779.

Sreelatha, A., Yee, S.S., Lopez, V.A., Park, B.C., Kinch, L.N., Pilch, S., Servage, K.A., Zhang, J., Jiou, J., Karasiewicz-Urbańska, M., et al. (2018). Protein AMPylation by an Evolutionarily conserved pseudokinase. Cell *175*, 809–821.e19.

Stadlmann, J., Taubenschmid, J., Wenzel, D., Gattinger, A., Dürnberger, G., Dusberger, F., Elling, U., Mach, L., Mechtler, K., and Penninger, J.M. (2017). Comparative glycoproteomics of stem cells identifies new players in ricin toxicity. Nature *549*, 538–542.

Stepien, B.K., Naumann, R., Holtz, A., Helppi, J., Huttner, W.B., and Vaid, S. (2020). Lengthening neurogenic period during neocortical development causes a hallmark of neocortex expansion. Curr Biol *30*, 4227–4237.e5. https://doi.org/10.1016/j.cub.2020.08.046.

Stoka, V., Turk, V., and Turk, B. (2016). Lysosomal cathepsins and their regulation in aging and neurodegeneration. Ageing Res. Rev. *32*, 22–37.

Truttmann, M.C., Pincus, D., and Ploegh, H.L. (2018). Chaperone AMPylation modulates aggregation and toxicity of neurodegenerative

disease-associated polypeptides. Proc. Natl. Acad. Sci. U S A *115*, E5008–E5017.

Tyanova, S., Temu, T., Sinitcyn, P., Carlson, A., Hein, M.Y., Geiger, T., Mann, M., and Cox, J. (2016). The Perseus computational platform for comprehensive analysis of (prote)omics data. Nat. Methods *13*, 731–740.

Yarbrough, M.L., Li, Y., Kinch, L.N., Grishin, N.V., Ball, H.L., and Orth, K. (2009). AMPylation of rho GTPases by *Vibrio* VopS disrupts effector binding and downstream signaling. Science *323*, 269–272.

Yu, X., and LaBaer, J. (2015). High-throughput identification of proteins with AMPylation using self-assembled human protein (NAPPA) microarrays. Nat. Protoc. *10*, 756–767.

Zanon, P.R.A., Lewald, L., and Hacker, S.M. (2020). Isotopically labeled desthiobiotin azide (isoDTB) tags enable global profiling of the bacterial cysteinome. Angew. Chem. Int. Ed. *59*, 2829–2836.

STAR★METHODS

KEY RESOURCES TABLE

REAGENT or RESOURCE	SOURCE	IDENTIFIER
Antibodies		
Goat polyclonal anti-mouse IgG, AF488-linked	Thermo Fisher Scientific	Cat# A-11001; RRID:AB_2534069
Goat polyclonal anti-rabbit IgG, AF488-linked	Thermo Fisher Scientific	Cat# A-11008; RRID: AB_143165
Goat polyclonal anti-rabbit IgG, HRP-linked	Sigma-Aldrich	Cat# A6667; RRID: AB_258307
Rabbit polyclonal anti-ABHD6	Thermo Fisher Scientific	Cat# PA5-38999; RRID AB_2555591
Rabbit polyclonal anti-ACP2	Thermo Fisher Scientific	Cat# PA5-29961; RRID: AB_2547435
Rabbit polyclonal anti-COX IV	Thermo Fisher Scientific	Cat# ab16056; RRID: AB_443304
Rabbit polyclonal anti-HSPA5	Thermo Fisher Scientific	Cat# PA5-34941; RRID: AB_2552290
Mouse monoclonal anti-KDEL (10C3)	Millipore	Cat# 420400; RRID: AB_212090
Mouse monoclonal anti-LAMP2 (H4B4)	DSHB	Cat# N/A; RRID: AB_528129
Rabbit polyclonal anti-PLD3	Sigma-Aldrich	Cat# HPA012800; RRID: AB_1855330
Mouse monoclonal anti-TUBB3	Sigma-Aldrich	Cat# T8660 RRID: AB_477590
Guinea pig polyclonal anti-DCX	Millipore	Cat# AB2253 RRID: AB_1586992
Rabbit polyclonal anti-TBR1	Millipore	Cat# AB31940 RRID: AB_2200219
Mouse polyclonal anti-MAP2	Millipore	Cat# AB5392 RRID: AB_2138153
Mouse monoclonal anti-Neun	Millipore	Cat# MAB377 RRID: AB_2298772
Goat polyclonal anti-mouse IgG2b, AF647-linked	Thermo Fisher Scientific	Cat# A-21242 RRID: AB_2535811
Goat polyclonal anti-rabbit IgG, AF546-linked	Thermo Fisher Scientific	Cat# A-11010 RRID: AB_2534077
Goat polyclonal anti-Guinea pig IgG, AF647-linked	Thermo Fisher Scientific	Cat# A-21450 RRID: AB_2735091
Goat polyclonal anti-mouse IgG, AF546-linked	Thermo Fisher Scientific	Cat# A-21123 RRID: AB_2535765
Mouse monoclonal anti-S100beta	Sigma-Aldrich	Cat# S2532 RRID: AB_477499
Rabbit polyclonal anti-FGFR3	Santa Cruz	Cat# sc-123 RRID: AB_631511
Goat anti-mouse IgG1, Alexa fluor 488	Thermo Fisher Scientific	Cat# A-21121 RRID: AB_2535764
Rabbit polyclonal anti-Ovalbumin	Thermo Fisher Scientific	Cat# PA5-97525 RRID: AB_2812141
Chemicals, peptides, and recombinant proteins		
Acetone (HPLC grade)	VWR chemicals	Cat# 200067.320; CAS: 67-64-1
Acetonitrile (LC-MS grade)	Fisher Scientific	Cat# A955-212; CAS: 75-05-8
Alanyl-Glutamine	Sigma-Aldrich	Cat# G8541, CAS: 39537-23-0
Ammoniumperoxodisulfat (APS)	Sigma-Aldrich	Cat# 09913; CAS: 7727-54-0
β-Mercaptoethanol	Sigma-Aldrich	Cat# M3148; CAS: 60-24-2

(*Continued on next page*)

Continued

REAGENT or RESOURCE	SOURCE	IDENTIFIER
Biotin-PEG_3-N_3	Carbosynth	Cat# FA34890 CAS: 875770-34-6
Bromphenol blue	Fluka	Cat# 32712 CAS: 115-39-9
BSA	AppliChem	Cat# A6588; CAS: 9048-46-8
Coomassie Blue R-250	Fluka	Cat# 27816; CAS: 6104-59-2
$CuSO_4$ x 5 H_2O	Acros	Cat# 10162, 7758-99-8
ddH2O (LC-MS grade)	Honeywell	Cat# 15350 CAS: 732-18-5
DMSO	Sigma-Aldrich	Cat# D4540, CAS: 67-68-5
Dithiothreitol	VWR (AppliChem)	Cat# A2948, CAS: 3483-12-3
Formic Acid (LC-MS grade)	Fisher Scientific	Cat# A117; CAS: 64-18-6
HEPES	Carl Roth	Cat# HN77.5; CAS: 7365-45-9
Iodacetamide	Sigma-Aldrich	Cat# I6125; CAS: 144-48-9
KCl	AppliChem	Cat# A2939; CAS: 7447-40-7
KH_2PO_4	Sigma-Aldrich	Cat# P9791; CAS: 7778-77-0
NA_2HPO_4	Sigma-Aldrich	Cat# T876; CAS: 7558-79-4
NA_2SeO_3	Sigma-Aldrich	Cat# S5261; CAS: 10102-18-8
NaCl	Bernd Kraft GmbH	Cat# KRAF04160; CAS: 7647-14-5
NP40	Sigma-Aldrich	Cat# 74385; CAS: 9016-45-9
Methanol (LC-MS grade)	Fisher Scientific	Cat# A456; CAS: 67-56-1
Powdered milk	AppliChem	Cat# A0830; CAS: 999999-99-4
SDS	AppliChem	Cat# A2572; CAS: 151-21-3
Sodium deoxycholate	Sigma-Aldrich	Cat# 30970; CAS: 302-95-4
TAMRA-N_3	Baseclick	CAT# BCFA-008-1
TBTA	TCI	Cat# T2993; CAS: 510758-28-8
TCEP	Carbosynth	Cat# FT01756; CAS: 51805-45-9
TEAB (1 M)	Sigma-Aldrich	Cat# T7408, CAS: 15715-58-9
TEMED	Sigma-Aldrich	Cat# T9281; CAS: 110-18-9
Thiourea	Merck	Cat# 107979; CAS: 62-56-6
Tris-base	Fisher Scientific	Cat# 10344; CAS: 77-86-1
Trypan Blue	Fisher Scientific	Cat# 11886
Tween® 20	VWR (AppliChem)	Cat# A4974; CAS: 9005-64-5
Urea	AppliChem	Cat# A1049, CAS: 57-13-6
DPBS (1×)	Sigma-Aldrich	Cat# D8357
DMEM (1×)	Sigma-Aldrich	Cat# D6546
Ham's F-12 w/o L-Glu	Sigma-Aldrich	Cat# N4888
cOmplete® protease inhibitor	Sigma-Aldrich	Cat# 05001
Normal goat serum	Biozol	Cat# VEC-S-1000
FCS	Thermo Fisher Scientific	Cat# A3840001
hHolo-transferrin	Sigma-Aldrich	Cat# 616424; CAS: 11096-37-0
hFGF-2	MACS Miltenyi Biotec	Cat# 130-104-921
hInsulin	BioXtra	Cat# I9278, CAS: 11061-68-0
hTGF- β1	MACS Miltenyi Biotec	Cat# 130-095-067
Geltrex	Thermo Fisher Scientific	Cat# A1413201
Immobilon® Western HRP sustrate	Merck Millipore	Cat# WBKLS0500
Color prestained protein standard, Broad range (10-250 kDa)	New England BioLabs	Cat# P7719S
Blue prestained protein standard, Broad range (11-250 kDa)	New England BioLabs	Cat# P7718L

(*Continued on next page*)

Continued

REAGENT or RESOURCE	SOURCE	IDENTIFIER
Pen-strep	Sigma-Aldrich	Cat# P0781
Rotiphorese.Gel 30 (37, 5:1)	Carl Roth	Cat# 3029.1
TrypLE express	Thermo Fisher Scientific	Cat# 12013
Trypsin	Promega	Cat# V5113
Thiazovivin	Merck Millipore	Cat# 420220; CAS: 1056-71-8
NeuroBrew-21	Miltenyi Biotech	Cat# 130-093-566
4,6-Diamidino-2-phenylindole	Sigma-Aldrich	Cat# D9542
Accutase	Stem Cell Technologies	Cat# 07920
Ascorbic acid	Sigma-Aldrich	Cat# A92902; CAS: 50-81-7
B27-supplement (minus vitamin A)	Thermo Fisher Scientific	Cat# 12010
BDNF	Peprotech	Cat# 450-02
dcAMP	Sigma-Aldrich	Cat# D1256; CAS: 93839-95-3
GDNF	Peprotech	Cat# 450-10
Laminin	Sigma-Aldrich	Cat# L2020; CAS: 114,956-81-9
Matrigel® Basement membrane matrix, LDEV-free	Corning®	Cat# 354234
Minimum essential medium/non-essential amino acid	Thermo Fisher Scientific	Cat# 11050
mTESR1 medium	Stem Cell Technologies	Cat# 85850
N2-supplement	Thermo Fisher Scientific	Cat# 17048
Neurobasal medium	Thermo Fisher Scientific	Cat# 21103049
Polyornithine	Sigma-Aldrich	Cat# P4957
Rock inhibitor Y-27632(2HCl)	Stem Cell Technologies	Cat# 72304
Astrocyte media	ScienCell	Cat# 1801
Recombinant human LIF	Alomone Labs	Cat# L-200
Recombinant human FGF-basic	Peprotech	Cat# AF-100-18 B
Recombinant human EGF	Peprotech	Cat# AF-100-15
Recombinant human noggin	Peprotech	Cat# 120-10C
Recombinant human PDGF-AA	R&D Systems	Cat# 221-AA
Accutase	Thermo Fisher Scientific	Cat# A1110501
Collagenase	Stem Cell Technologies	Cat# 07909
Critical commercial assays		
Pierce® BCA protein Assay kit	Thermo Fisher Scientific	Cat# 23225
Deposited data		
MS raw data and calculation results	ProteomeXchange	PXD023873
Experimental models: Cell lines		
Human: HeLa	Puck and Marcus, 1955	RRID: CVCL_0030
Human: SH-SY5Y	Biedler et al., 1973	RRID: CVCL_0019
Human: iNGNs	Volker Busskamp, CRTD Dresden	
Human: iPSCs	Dr.Micha Drukker HHZ Munich	HMGU No 1 RRID: CVCL_YT30
Software and algorithms		
MaxQuant	Cox et al., 2014	https://www.maxquant.org/download_asset/maxquant/latest
Perseus	Tyanova et al., 2016	https://maxquant.net/download_asset/perseus/latest
Origin	NA	https://www.originlab.com/

RESOURCE AVAILABILITY

Lead contact

Further information and requests for resources and reagents should be directed to and will be fulfilled by the Lead Contact, Dr. Pavel Kielkowski (pavel.kielkowski@cup.lmu.de).

Materials availability

This study did not generate new unique reagents.

Data and code availability

- Mass spectrometry-based proteomics data have been deposited at ProteomeXchange and are publicly available as of the date of publication. The accession number is listed in the key resources table.
- This paper does not report original code.
- Any additional information required to reanalyze the data reported in this paper is available from the lead contact upon request.

EXPERIMENTAL MODEL AND SUBJECT DETAILS

iNGN cells

Coating of petri dishes for iNGN culturing. In order to culture iNGNs, petri dishes have to be coated. For this, 15 mg/mL Geltrex LDEV-free was diluted 1:1000 in cold coating media (49.5% DMEM (1×), 49.5% F-12, 1 % Pen-Strep 100×) and was immediately added onto the petri dish. The coating volumes were as follows: p60, 3.5 mL; p100, 10 mL and p150, 25 mL. After addition of the coating media to the petri dishes, they were incubated at least one hour in the incubator at 37°C and were then ready for use.

Passaging and culturing of iNGN cells in p100 dish. First, media was removed and cells were washed with 4 mL PBS. Then, 1.5 mL TrypLE^{TM} Express was added and the mixture was incubated 7 min at 37°C. The detached cells were resuspended with 2 mL pre-warmed E7 media (49% (v/v) DMEM, 49% (v/v) F-12, 1% (v/v) Alanyl-Glutamine 100×, 77.6 nM Na_2SeO_3, 11.2 mM NaCl, 10 μg/mL hHolo-Transferrin, 10 μg/mL hInsulin) supplemented with 2 μM thiazovivin (E7+TZ) and the cell suspension was transferred to a 15 mL falcon. Before the cell suspension was spinned down 5 min at 600 rpm, the concentration of the cell suspension was determined by mixing 10 μL cell suspension with 10 μL trypan blue. Afterwards, the supernatant was removed and the cell pellet was resuspended in the calculated amount of media to obtain a concentration of 1.5 million cells in 1 mL (For seeding iNGNs for differentiation the concentration was adjusted to 2.5 million cells in 1 mL). Next, the media of the previously coated p100 dish was removed and 9 mL E7+TZ media was added and topped with 1 mL of the cell suspension. Finally, the E7+TZ media was supplemented with 10 μL TGF-beta (2.0 μg/mL) and 10 μL FGF-IS (20 μg/mL) in order to obtain E9+TZ medium. The iNGN cells were cultured overnight at 37°C and 5% CO_2, before the media was exchanged to E9 on the next day.

Differentiation of iNGNs in p100 dish. In order to differentiate iNGNs to neurons during 4 days, the expression of the two transcriptions factors Neurogenin-1 and Neurogenin-2 have to be induced by the addition of doxycycline (Dox). For this, 2.5 million cells in 10 mL E7 media containing 0.5 μg/mL Dox and 2 μM TZ (E7+Dox + TZ) were seeded in a p100 dish. After overnight incubation at 37°C in the incubator, the media was exchanged to 10 mL E7+Dox without TZ. On the next day, 10 mL fresh E7+Dox media was added onto the dish. On day 4, half of the E7+dox media was removed and 5 mL Neurobasal A media supplemented with 4% NS-21 was added. On day 5, the complete media was removed and 10 mL Neurobasal A media supplemented with 2% NS-21 and 2 mM L-alanyl-glutmanine was added. On day 7, 2 mL of the media was removed and 2 mL Neurobasal A media supplemented with 2% NS-21 and 2 mM L-alanyl-glutmanine was added. Until day 10, the iNGNs were incubated at 37°C in the incubator without any further media exchange.

iPSC culture for physiological neurons differentiation. iPSCs (RRID: CVCL_YT30) were cultured as previously described in (Ayo-Martin et al., 2020). They were cultured in Matrigel Basement Membrane Matrix, LDEV-free coated plates in mTESR1 medium supplemented with 1× mTESR1 supplement. Media was changed every day. For passaging, the cells were dissociated using Accutase and the collected colonies

were resuspended in mTESR1 with 1× mTESR1 supplement and 10 μM Rock inhibitor Y-27632(2HCl) and diluted in the desired density.

Generation of NPCs

Neural progenitors were generated as previously described with modifications (Boyer et al., 2012; Klaus et al., 2019). In short, embryoid bodies were generated from iPSCs by plating colonies in suspension in neural induction medium consisting of DMEM F12 with N2 and B27 supplements (minus vitamin A). After 7 days in suspension, Embryoid bodies were plated on polyornithine and laminin coated dishes and cultured for 7 days in neural induction medium. Neural rosettes were manually picked, dissociated and plated in a new polyornithine/laminin-coated plate in neural progenitor medium (neural induction medium supplemented with bFGF at 20 ng/mL). For passaging, the cells were dissociated using Accutase and split at a maximum ratio of 1:4.

Generation of neurons

Neurons were generated following the Gunhanlar protocol (Gunhanlar et al., 2018). Briefly, NPCs were plated on poly-L-ornithine and laminin coated dishes in neural differentiation medium consisting of Neurobasal with N2, B27 supplements (minus vitamin A), minimum essential medium/non-essential amino acid and laminin, supplemented with BDNF, GDNF, ascorbic acid and dcAMP. Media was changed every 2–3 days. Young and mature neurons were collected after 5 weeks and 10 weeks in culture respectively.

iPSC culture for astrocytes differentiation

iPSCs were cultured on Geltrex LDEV-Free, Reduced Growth Factor Basement Membrane Matrix coated 6-well plates in mTESR1 medium supplemented with 1× mTESR1 supplement. Media was changed every day. For passaging, the cells were incubated with Collagenase Type IV for 5–7 minutes at 37°C. The collagenase was aspirated and fresh mTESR1 with 1× mTESR1 supplement was added to each well. A cell scraper was used to collect the cells, and they were subsequently plated on a fresh 6-well plate at the desired dilution.

Generation of GPCs and astrocytes

Glial progenitor cells and astrocytes were generated as previously described with modifications (Santos et al., 2017). Briefly, confluent iPSC cultures were dissociated with collagenase, collected with a cell scraper and then cultured in suspension to form embryoid bodies. The first 24hrs the cells were cultured in mTESR1 with 1× mTESR1 supplement and 10 μM Rock inhibitor Y-27632. For the next two weeks the cells were cultured in Astrocyte medium (AM) supplemented with 20ng/mL Noggin and 10 ng/mL PDGFAA, and an additional week with only PDGFAA. The embryoid bodies were then manually dissociated by pipetting and the resulting GPCs were plated on poly-L-ornithine and laminin-coated dishes in AM supplemented with 10ng/mL bFGF and 10ng/mL EGF. Astrocytes were differentiated from GPCs in AM supplemented with 10ng/mL LIF. Media was changed every other day. The GPCs and astrocytes were collected after 5 weeks and 9 weeks of differentiation respectively. The images were obtained on a LSM710 laser-scanning confocal (Carl Zeiss microscope, ZEN software) at ×40 magnification.

Culturing of HeLa and SH-SY5Y cells

HeLa (RRID: CVCL_0030) and SH-SY5Y (RRID: CVCL_0019) cells were cultured in Dulbeccos Modified Eagles Medium – high glucose (DMEM) supplemented with 10% fetal calf serum (FCS) and 2 mM L-alanyl-glutamine at 37°C and 5% CO_2 atmosphere.

METHOD DETAILS

Fluorescence imaging

SH-SY5Y neuroblastoma cells were seeded on glass coverslips and grown in DMEM supplemented with 10% FCS. For Click staining of AMPylated proteins, cells were treated with 100 μM pro-N6pA for 24 h. After washing twice in cold PBS, the cells were fixed with 4% paraformaldehyde (PFA) in PBS for 20 min, washed two more times in PBS and permeabilized by incubation with 0.1% Triton X-100 in PBS for 5 min. The metabolically labelled proteins were coupled to TAMRA via CuAAC using 1 mM $CuSO_4$, 5 mM THPTA, 10 μM TAMRA-N_3 and 100 mM sodium ascorbate in PBS for 1 h. Following washing twice, a second fixation in 4% PFA for 10 min and two more washing steps. For immunostaining, the cells were permeabilized in 0.2% saponin in PBS for 5 min, followed by quenching with 0.12% glycine and 0.2% saponin for 10 min

and incubation in blocking solution for 1 h (10% FCS and 0.2% saponin in PBS). Primary antibodies were diluted in blocking solution and incubated with the coverslips overnight at 4°C. After four washing steps in 0.2% saponin, the cells were incubated with AlexaFluor488 coupled secondary antibodies for 1 h at room temperature, washed four times in 0.2% saponin and twice in H_2O. The coverslips were finally placed in 15 μL mounting medium (167 mg/mL Mowiol 4–88, 3% glycerol, 20 mg/mL DABCO, 1 μg/mL DAPI in PBS) Microscopic images were recorded at an Olympus FV1000 confocal laser scanning microscope using a U Plan S-Apo 100× oil objective (1.40 NA).

Immunoistochemistry – physiological neurons

10 weeks old mature neurons were fixed using 4% PFA for 10 min and permeabilized with 0.3% Triton for 5 min. After fixation and permeabilization, cells were blocked with 0.1% Tween, 10% Normal Goat Serum. Primary and secondary antibodies were diluted in blocking solution. Nuclei were visualized using 0.5 mg/mL 4,6-diamidino-2-phenylindole (DAPI). Stained cells were analyzed using a Leica laser-scanning microscope.

PLD3 activity assay

For quantitative determination of PLD3 5'exonuclease activity, lysates were prepared in TRIS-lysis buffer (TBS with 1% (v/v) Triton X-100 and 1 tablet cOmplete EDTA-free protease inhibitor cocktail). After collecting the whole cell lysates as described above, lysates were diluted in a final volume of 100 μL MES reaction buffer (50 mM MES, 200 mM NaCl) to a final concentration of 50 ng/μL in a lumox multiwell 96 plate (Sarstedt). The reaction was started by addition of 100 pmol quenched FAM-ssDNA substrate (6-FAM-AC CATGACGTTC*C*T*G*-BMN-Q535 (Biomers.net) with * indicating a phosphothioate bond). After a pre-incubation period of 30 min fluorescence emission at 528 nm (following excitation at 485 nm) was measured in a microwell plate reader (SynergyHT from BioTek) from below the wells over a period of 12 h every 5 min while incubation at 37°C. For evaluation, a substrate control without lysate and a lysate control without substrate were measured together with the samples. The 5'exonuclease activity was calculated as the slope of the measured fluorescence in the samples minus both controls.

Chemical proteomics

Seeding of iNGNs for differentiation. The identification of the AMPylation targets during neuronal differentiation was performed with four controls and four probe treated samples for each time point. In each 10 cm dish 2.5 million iNGNs in 10 mL E7+Dox+TZ media were seeded for differentiation. The media composition that is used for each day of differentiation is described in the section above, differentiation of iNGNs. One day before the cells were harvested, the samples were treated with 5 μL of 100 mM AMPylation probe (pro-N6pA) and the controls with 5 μL DMSO.

Harvesting and cell lysis. Cells were washed twice with 2 mL PBS. Then, 500 μL lysis buffer (PBS with 1% (v/v) NP40 and 1% (w/v) sodium deoxycholate and 1 tablet protease inhibitors per 10 mL buffer)) was added and cells were scrapped into an Eppendorf tube. The cell suspension was incubated 15 min at 4°C with agitation, before cells were spinned down 10 min at 12,000 rpm and 4°C. Subsequently, the cytosolic fraction of the lysate was transferred into a new 2 mL Eppendorf tube.

Measurement of protein concentrations. In order to measure the protein concentrations of the lysates bicinchoninic acid assay was performed. First, bovine serum albumin (BSA) standards with concentrations of 12.5, 25, 50, 100, 200 and 400 μg/mL were prepared and samples as well as controls were diluted 40 times to a total volume of 200 μL. To measure standards, samples and controls in triplicates, 50 μL of each was added to three wells of a transparent 96-well plate with flat bottom. Afterwards, 100 μL working reagent (2 μL R2 and 98 μL R1) was added to each well by a multistepper and the plate was incubated 15 min at 60°C. Then, the absorbance at 620 nm was measured by Tecan and the protein concentrations were calculated. For each replicate, except for the 24 h time point (250 μg), 400 μg of protein was used and the volumes were adjusted to a total volume of 970 μL with 0.2% SDS in PBS.

Coupling of AMPylated proteins. In order to couple the alkyne residue of AMPylated target proteins with Biotin-PEG_3-N_3, CuAAC was used. For this reaction, 10 μL 10 mM Biotin-PEG_3-N_3, 10 μL 100 mM TCEP and 1.2 μL 83.5 mM TBTA were added to 970 μL of each lysate. The mixture was vortexed and spinned down before 20 μL 50 mM $CuSO_4$ was added to initiate the reaction. Finally, the reaction mixture was incubated 1.5 h shaking at 600 rpm and 25°C in the dark.

Protein precipitation. First, each reaction mixture of the previously performed click reaction was transferred to a 15 mL falcon. Then, 4 mL acetone was added to each falcon in order to precipitate the proteins. After 1 h of incubation at −20°C, proteins were spinned down 15 min at 11,000 rpm and 4°C. Supernatant was discarded and each pellet was resuspended in 1 mL methanol by sonicating 3 times for 5 s at 20% intensity. Subsequently, each suspension was transferred to a 1.5 mL Eppendorf tube and was centrifuged 10 min at 11,000 rpm and 4°C. Each pellet was washed again with 1 mL methanol before it was dissolved in 1 mL 0.2% SDS in PBS by sonicating 3 times for 5 s at 20% intensity.

Avidin beads enrichment. In order to enrich the biotinylated proteins, avidin agarose beads (Sigma-Aldrich) were used. First, avidin beads were thawed on ice before 50 µL avidin bead suspension for each sample or control was washed 3 times with 1 mL 0.2% SDS in PBS to equilibrate the beads. After each addition of washing solution, the Eppendorf tube was carefully inverted 10 times, the suspension was centrifuged 2 min at 2000 rpm at room temperature and the supernatant was discarded. Subsequently, each dissolved protein pellet was spinned down at maximum speed for 2 min and room temperature before the supernatant was added to the equilibrated beads. After each avidin bead suspension was incubated 1 h under continuous mixing at room temperature, the beads of each sample or control were washed 3 times with 1 mL 0.2% SDS in PBS, 2 times with 1 mL 6 M urea in H_2O and 3 times with 1 mL PBS.

On beads digest of enriched proteins. In order to prepare defined peptide fragments for the following MS-measurements, the enriched proteins were digested with trypsin. First, the washed avidin beads were resuspended in 200 µL Xbuffer (7 M urea, 2 M thiourea in 20 mM HEPES pH 7.5). Then, 0.2 µL 1 M DTT was added to reduce the disulfide bonds. Afterwards, each mixture was vortexed and incubated 45 min at room temperature shaking at 600 rpm. Next, 2 µL 550 mM IAA was added to alkylate the cysteine residues. After each mixture was vortexed and incubated 30 min at room temperature shaking at 600 rpm in the dark, 0.8 µL 1 M DTT was added to quench the alkylation. Subsequently, each mixture was vortexed and incubated for another 30 min at room temperature shaking at 600 rpm in the dark before 600 µL 50 mM TEAB was added to increase the pH value to 8. Afterward, 1.5 µL trypsin (0.5 µg/µL in 50 mM acetic acid) was added to digest the enriched proteins. Finally, each mixture was vortexed and incubated overnight at 37°C shaking at 600 rpm.

On the next day, 4 µL FA was added to stop the digest. Subsequently, each mixture was vortexed and centrifuged 1 min at 2000 rpm before the supernatant was transferred into a new Eppendorf tube. After 50 µL 0.1% FA was added to the avidin beads, each mixture was vortexed, the centrifugation step was repeated and the supernatant was again transferred to the new Eppendorf tube. Then, 50 µL 0.1% FA was added once more to the avidin beads and each mixture was vortexed. Finally, each mixture was centrifuged 3 min at 13,000 rpm and the supernatant was transferred to the new Eppendorf tube as before. For the following desalting step of the digested proteins, the pH was checked to be below 3.

Desalting of peptides mixture. In order to remove all disturbing salt from the digested proteins, Sep Pak C18 cartridges (50 mg columns, waters) were used. First, cartridges were washed with 1 mL ACN and 1 mL 80% ACN with 0.5% FA. Then, cartridges were equilibrated with 3 mL 0.5% FA before the acidified samples were loaded slowly. Afterwards, cartridges were washed with 3 mL 0.5% FA. The desalted peptides were eluted 2 times with 250 µL 80% ACN with 0.5% FA into a LoBind Eppendorf tube. Finally, the eluates were lyophilized.

Final peptide preparation. First, 30 µL 1% FA was added to the lyophilized peptides. Then, the mixture was vortexed, spinned down and sonicated 15 min to dissolve the complete peptides. Afterwards, the dissolved peptides were spinned down and added onto centrifugal filter units. Finally, the solution was centrifuged 1 min at 13,000 rpm and the filtrate was transferred into plastic MS vials.

MS-measurement. MS-measurements were performed on a Q Exactive HF mass spectrometer (Thermo Fisher Scientific) coupled to an UltiMate™ 3000 Nano HPLC (Thermo Fisher Scientific) via an EASY-Spray source (Thermo Fisher Scientific). First, peptides were loaded on a Acclaim PepMap 100 µ-precolumn cartridge (5 µm, 100 Å, 300 µm ID × 5 mm, Thermo Fisher Scientific). Then, peptides were separated at 40°C on a PicoTip emitter (noncoated, 15 cm, 75 µm ID, 8 µm tip, New Objective) that was in house packed with Reprosil-Pur 120 C18-AQ material (1.9 µm, 120 Å, Dr. A. Maisch GmbH). The gradient was run from 1-36% ACN supplemented with 0.1% FA during a 120 min method (0–5 min 1%; 5-8 min to 6%; 8-98 min to 36%; 98-100 min to 85%; 100–105 min wash with 85%; 105-110 min to 1%, 110–120 min with 1%) at a flow rate of

200 nL/min. For measurements of chemical-proteomic samples on Q Exactive HF mass spectrometer, the following settings were used: The Q Exactive HF was operated in dd-MS^2 mode with the following settings: Polarity: positive; MS^1 resolution: 120 k; MS^1 AGC target: 3×10^6 charges; MS^1 maximum IT: 20 ms; MS1 scan range: m/z 300–1750; MS^2 resolution: 15 k; MS^2 AGC target: 2×10^5 charges; MS^2 maximum IT: 100 ms; Top N: 20; isolation window: m/z 1.6; isolation offset: m/z 0.2; HCD stepped normalised collision energy: 28%; intensity threshold: 5×10^4 counts; charge exclusion: unassigned, 1, 7, 8, >8; peptide match: off; exclude isotopes: on; dynamic exclusion: 90 s.

Full proteome analysis. In order to quantify the proteins levels during neuronal differentiation, a full proteom analysis was performed. For this approach, the same lysates (control samples) that were used for the chemical proteomic experiments were used. First, 100 µg protein of each lysate was diluted to a total volume of 200 µL with 0.2% SDS in PBS. Then, 800 µL acetone was added and incubated 1 h at – 20°C to precipitate proteins. Next, proteins were spinned down 15 min at 11,000 rpm and 4°C and the supernatant was discarded. Each pellet was resuspended in 1 mL methanol by sonicating 3 times for 5 s at 20% intensity and the mixture was spinned down once again as before. The supernatant was discarded and the washed protein pellets were dissolved in 200 µL Xbuffer. The following digest and desalting were performed as described in the sections above. Finally, the lyophilized peptides were dissolved in 200 µL 1% FA and filtered as described in the section, final peptide preparation.

Phosphatase treatment. In order to ensure that we only observed the separation of AMPylated and not phosphorylated proteins using a Phos-tag gel, the lysates were treated with a phosphatase prior to analysis. For the reaction, 10 µL 10× buffer (0.5 M Tris, 0.1 M $MgCl_2$, pH 9.0), 1 µL shrimp alkaline phosphatase (1000u/mL) and 100 µg lysate were mixed and filled up with H_2O to a total volume of 100 µL. The reaction mixture was incubated overnight at 37°C. As a positive control, the phosphorylated protein ovalbumin was used.

Western blot analysis. For each Western blot analysis, 20 µg cell lysate was used. In order to denature proteins, 4 µL 5× Lämmli buffer (10% (w/v) SDS, 50% (v/v) glycerol, 25% (v/v) β-mercaptoethanol, 0.5% (w/v) bromphenol blue, 315 mM Tris/HCl, pH 6.8) was added to 16 µL lysate solution and the samples were boiled 5 min at 95°C. Afterwards, 20 µL of each sample was loaded onto a 7.5, 10 or 12.5% SDS gel and proteins were separated according to their size by SDS-PAGE. Then, the separated proteins were transferred onto a membrane using a blotting sandwich moistened by blotting buffer (48 mM Tris, 39 mM glycine, 0.0375% (m/v) SDS, 20% (v/v) methanol), which was composed of one extra thick blot paper, the PVDF transfer membrane, the SDS-PAGE gel and again one extra thick blot paper. Before the protein transfer was carried out 45 min at 25 V using a Semi Dry Blotter (Bio-Rad), the transfer membrane was pre-incubated 5 min in methanol. In order to block non-specific binding sites, the membrane was incubated 60 min in blocking solution (0.5 g milk powder in 10 mL PBST (PBS +0.5% Tween)). Subsequently, 10 µL primary antibody with specificity for the protein of interest was added and the mixture was incubated 1 h at room temperature. The membrane was washed 3 times for 10 min with PBST before 1 µL of the secondary HRP antibody in 10 mL blocking solution was added. After 1 h of incubation at room temperature the membrane was washed again 3 times for 10 min with PBST. Then, 400 µL ECL Substrate and 400 µL peroxide solution were mixed and added to the membrane to stain the Western blot. Finally, images of the Western blot were taken by developing machine Amersham Imager 680 (GE Healthcare).

Phos-tag gel. In order to separate the unmodified from the post-translationally modified protein form, a Phos-tag gel was used. Compared to conventional SDS-gels, Phos-tag gels contain additionally Phos-tag reagent and $MnCl_2$. To pore a 1 mm thick 7.5% Phos-tag separating gel, 1.25 mL 30% acrylamide solution, 1.25 mL 1.5 M Tris pH 8.8 solution, 50 µL 5 mM Phos-tag reagent, 50 µL 10 mM $MnCl_2$, 50 µL 10% SDS, 2.33 mL H_2O, 5 µL TEMED and 25 µL 10% APS were mixed. The stacking gel was prepared as for conventional SDS-gels by mixing 0.6 mL 30% acrylamide solution, 1 mL 0.5 M Tris pH 6.8 solution, 40 µL 10% SDS, 2.34 mL H_2O, 4 µL TEMED and 20 µL 10% APS. After the Phos-tag gel was polymerized, 20 µg of the lysates were loaded and dependent on the size of the protein of interest, the gel was run for 2 to 3 h at 150 V. Following the separation, the gel was washed 2 times 15 min with blotting buffer (48 mM Tris, 39 mM glycine, 0.0375% (m/v) SDS, 20% (v/v) methanol) supplemented with 10 mM EDTA to remove the manganese-ions. Subsequently, the gel was washed 15 min in blotting buffer before it was blotted as described in the Western blot section.

QUANTIFICATION AND STATISTICAL ANALYSIS

Calculation chemical proteomics

MS Raw files were analysed using MaxQuant software 1.6.12.0 with the Andromeda search engine. Searches were performed against the Uniprot database for Homo sapiens (taxon identifier: 9606, March 2020). At least two unique peptides were required for protein identification. False discovery rate determination was carried out using a decoy database and thresholds were set to 1% FDR both at peptide-spectrum match and at protein levels. LFQ quantification was used as described for each sample.

Statistical analysis chemical proteomics

Statistical analysis of the MaxQuant result table proteinGroups.txt was done with Perseus 1.6.10.43.

First, LFQ intensities were $\log_2$-transformed. Afterwards, potential contaminants as well as reverse peptides were removed. Then, the rows were divided into two groups - DMSO (control) and probe treated sample (sample). Subsequently, the groups were filtered for at least three valid values out of four rows in at least one group and the missing values were replaced from normal distribution. The $-\log_{10}$(p values) were obtained by a two-sided one sample Student's t-test over replicates with the initial significance level of $p = 0.05$ adjustment by the multiple testing correction method of Benjamini and Hochberg (FDR = 0.05) using the volcano plot function.

Profile plots

In order to visualize the changes of the LFQ-intensities during the iNGN differentiation, profile plots were used. For this, the mean (circle), the median (line) and the whiskers for outliers from $n = 4$ of each time point were prepared in Origin with box defined by 25^{th} and 75^{th} percentile.